Observation of intracavity electromagnetically induced transparency in Cs vapor coupled with a standing-wave cavity

**Haitao Zhou (周海涛)*, Shaona Che (车少娜), Pengcheng Zuo (左鹏程),
Yuhong Han (韩宇宏), and Dan Wang (王 丹)**

College of Physics and Electronics Engineering, Shanxi University, Taiyuan 030006, China
*Corresponding author: zht007@sxu.edu.cn

The cavity transmission spectrum is experimentally investigated in Λ-type three-level atoms coupled to a standing-wave cavity system. It is shown that the dark-state polariton peak is not generated at resonance but rather at off-resonance. The theoretical analysis reveals that the absence of an on-resonance dark-state polariton peak is mainly caused by the strong absorption of the intracavity medium to the probe cavity mode counterpropagating with the coupling field due to the Doppler shift in the hot atoms. Moreover, the optimal frequency position of the cavity mode for an efficient dark-state polariton peak is also demonstrated.

Cavity quantum electrodynamics (QED)[1–3] is mainly researching the interaction process with a coherent atomic medium placed inside an optical resonant cavity, and has been of great interest in recent years. A well-known cavity-QED effect is the vacuum Rabi splitting or normal-mode splitting phenomenon that is under the strong coupling condition, where the cavity transmission spectrum exhibits a double-splitting-peaked profile when two-level atoms are coupled into a single cavity mode[4–7]. Based on the above, when strong coherent light is injected into the intercavity medium to form a Λ-type three-level structure in which the electromagnetically induced transparency (EIT) is prepared[8,9], the cavity transmission spectrum produces an additional narrow central peak under the condition of the two-photon resonance, that is the intercavity EIT (i.e., dark-state polariton)[10]. Possible applications of intracavity EIT include long-lived storage of quantum information[11], preparation of squeezed or entangled states[12,13], and high-resolution spectroscopy[14,15]. The three-peak spectrum of a three-level EIT atom-cavity system has been demonstrated in cold atoms[16,17], single atoms[18], hot atomic vapor[19,20], and ion Coulomb crystals[21,22]. The EIT effect was also achieved with a terahertz frequency in a waveguide cavity and meta-atoms[23–25]. Recently, the four-wave mixing effect[26,27] based on the atom-cavity system has also been researched[28–31]. However, the spectrum property of the hot three-level atom standing-wave cavity (SC) system has not been reported yet.

As the resonant probe mode is copropagating with the coupling field for the composite system with hot Λ-type three-level atoms inside a ring cavity (RC), which is Doppler free for the intracavity moving atoms to the probe mode and coupling frequency, the intracavity EIT is achieved at the center of atomic resonance when the two-photon resonance is satisfied[20]. In this Letter, we experimentally demonstrate the cavity transmission spectrum in a hot Cs vapor coupled to a near-confocal standing-wave cavity (SC) by controlling the frequency detunings of the coupling field and the cavity-mode field. Quite different from the situation of an optical RC[19], however, it is shown that the dark-state polariton peak is created not at the center of atomic resonance but rather at off-resonance. Theoretically, the Doppler-shift effect due to the hot atoms and the coherent pump effect of the coupling fields[9,18] can give a qualitative interpretation. Furthermore, the multipeak profiles and their position distributions relevant to the frequency detunings of the cavity mode and the coupling field are also experimental investigated.

The energy levels and experimental setup are shown in Fig. 1. The hyperfine structure in the D1 line of the ^{133}Cs atom is used for the Λ-type three-level EIT system[26] composed of two lower states $|a\rangle$ ($6^2S_{1/2}, F = 4$), $|b\rangle$ ($6^2S_{1/2}, F = 3$), and a common upper state $|c\rangle$ ($6^2P_{1/2}, F = 4$) [see Fig. 1(a)]. The coupling and probe fields drive the transitions $|a\rangle\leftrightarrow|c\rangle$ and $|b\rangle\leftrightarrow|c\rangle$ with frequencies ω_p and ω_c and detunings $\Delta_p = \omega_p - \omega_{ca}$ and $\Delta_c = \omega_c - \omega_{cb}$, respectively. ω_{ca} and ω_{cb} are the corresponding resonance frequency. A near-confocal optical SC is composed of an input mirror M1 and an output mirror M2 that have the same transmissivity ($T_{M1} = T_{M2} = 0.5\%$) and the curvature radius ($\rho_{M1} = \rho_{M2} = 150$ mm). A piezoelectric transducer (PZT) mounted on M2 is used for scanning and locking the cavity length. The Cs vapor cell is 75 mm long with antireflection (AR) coated end windows and is wrapped in μ-metal sheets for magnetic field shielding and heat tape for controlling its temperature. The vertical-polarized coupling field is injected through a polarization beam splitter
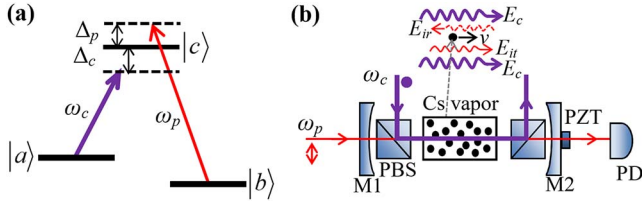
Fig. 1. (a) The Λ-type three-level scheme. (b) The experimental setup. M1 and M2, plane-concave mirrors. The polarization of the probe is horizontal and that of the coupling is vertical.

(PBS), and is reflected out by another PBS to avoid circulating in the cavity. The horizontal polarized probe beam is injected into the cavity via the input mirror M1 and circulates in the cavity as the cavity field, and the transmission signal is detected by a photodiode detector (PD). The waist diameter of the coupling and the probe fields at the center of the vapor cell are estimated to be 300 and 146 µm, respectively. When the vapor cell and two PBSs are included in the confocal caivity, the cavity finesse decreases from 600 to 31.

Figure 2 plots the experimentally measured cavity transmission spectra versus the probe frequency detuning Δ_p. When there is no coupling work ($P_c = 0$), the cavity transmission shows a three-peak profile, which includes two normal splitting modes and the residual resonant transmission peak for the qth cavity mode exactly at the atomic resonance ($\delta_q = 0$)[32], δ_q is defined as the q'th cavity-mode detuning [see the red curve (I) in Fig. 2]. When the coupling beam is injected and its power is $P_c = 10$ mW, the splitting of the two near-symmetric normal side peaks becomes larger because the interaction strength of atom-cavity increases from $\sqrt{g^2 N}$ to $\sqrt{g^2 N + \Omega_c^2/4}$[18], where g is the single-atom-cavity coupling strength, N is the number of atoms in the cavity-mode volume, and Ω_c is the Rabi frequency of the coupling beam. Quite different from the results of the RC[17], however, the dark-state polariton peak is not seen in
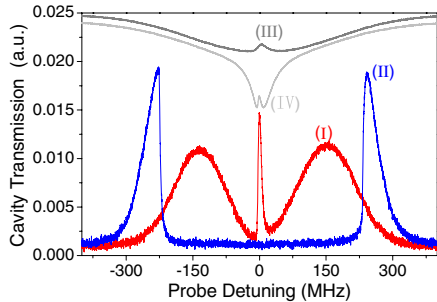

Fig. 2. (Color online) Cavity transmission spectrum versus the probe detuning in the different coupling powers at single-photon resonance ($\Delta_c = 0$): (I) $P_c = 0$ (red solid line); (II) $P_c = 10$ mW (blue solid line). (III) and (IV) are the SAS (gray line) and EIT (light gray line) signals in free space, respectively. The other experimental parameters are: $T = 35°C$, $P_p = 4$ mW.

the resonant case ($\delta_q = \Delta_c = 0$) [see the blue curve (II) in Fig. 2]. This is mainly because the cavity mode is reciprocating in the SC, rather a strong absorption not transparency for the probe cavity mode reflected by M2 couterpropagating with the coupling beam, restrains the creation of the dark-state polariton peak [see Fig. 1(b)]. The relative discussion is seen at the next section. As the cavity transmission is detected by scanning the probe frequency with a fixed cavity length, we use the saturated absorption spectrum (SAS) to judge the frequency scanning range of the probe [see the gray curve (III) in Fig. 2]. Furthermore, the little peak of the light gray curve (IV) is the EIT signal obtained by detecting the transmission of the probe acting with the Cs vapor coupled by the co-propagating coupling field in free space (not plotted in the experimental setup in Fig. 1), which is generated under the condition of two-photon resonance ($\Delta_c = \Delta_p$) and can be used to monitor the frequency detuning of the coupling beam.

Theoretically, much attention is focused on why the dark-state polariton peak can be seen at a certain coupling detuning not close to the center of atomic resonance for a composite SC. So, the susceptibility of the intracavity atoms should be considered primarily under the free space condition. See Fig. 1(a) for a Λ-type three-level system, the density-matrix equations of motion in the rotating frame are given by[33]

$$
\rho_{aa} + \rho_{bb} + \rho_{cc} = 1,
$$
$$
\dot{\rho}_{aa} = \gamma_{ca}\rho_{cc} + b(\rho_{bb} - \rho_{aa}) - i\Omega_p(\rho_{ac} - \rho_{ca}),
$$
$$
\dot{\rho}_{bb} = \gamma_{cb}\rho_{cc} + b(\rho_{aa} - \rho_{bb}) - i\Omega_c(\rho_{bc} - \rho_{cb}),
$$
$$
\dot{\rho}_{ca} = -(i\Delta_p + \Gamma_{ca})\rho_{ca} + i\Omega_c\rho_{ba} - i\Omega_p(\rho_{cc} - \rho_{aa}),
$$
$$
\dot{\rho}_{cb} = -(i\Delta_c + \Gamma_{cb})\rho_{cb} + i\Omega_p\rho_{ab} - i\Omega_c(\rho_{cc} - \rho_{bb}),
$$
$$
\dot{\rho}_{ab} = (i\Delta_p - i\Delta_c - \Gamma_{ab})\rho_{ab} + i\Omega_p\rho_{cb} - i\Omega_c\rho_{ac}, \quad (1)
$$

where γ_{ca} and γ_{cb} are the decay rates from level $|c\rangle$ to $|a\rangle$ and $|b\rangle$, respectively; Ω_p and Ω_c are the Rabi frequencies of probe and coupling fields, respectively; the off-diagonal decay rates are $\Gamma_{ij} = \gamma_{ij} + \gamma_{ii}$, γ_{ii} is the dephasing rate of level i; and b is the population relaxation rates between $|a\rangle$ and $|b\rangle$.

It is expressed by solving the Eqs. (1) for ρ_{ca} in a steady state

$$
\rho_{ca} = \frac{i\Omega_p\{(-i\Delta_c + \Gamma_{cb})[i(\Delta_c - \Delta_p) + \Gamma_{ab}]\rho_{bb} - \rho_{cc}\Omega_c^2\}}{(-i\Delta_c + \Gamma_{cb})\{[i(\Delta_c - \Delta_p) + \Gamma_{ab}](i\Delta_p + \Gamma_{ca}) + \Omega_c^2\}}, \quad (2)
$$

considering the Doppler-broadening effect of the intercavity atoms, the susceptibility of the system for probe laser χ expresses the ρ_{ca} as a function of the Doppler shift v, and integrate over the Maxwell-velocity distribution $f(kv)$,

$$
\chi = \int_{-\infty}^{\infty} d(kv) h \frac{\rho_{ca}}{\Omega_p} f(kv), \quad (3)
$$

where $f(kv) = (ku\sqrt{\pi})^{-1} \exp[-(kv)^2/(ku)^2]$, k is the wave vector, $u = \sqrt{2k_B T/m}$ is the most probable speed of an atom at a given temperature T and atomic mass m, k_B is the Boltzmann constant, $h = N\sigma^2/\epsilon_0\hbar$ is a constant, and N is the atomic density at temperature T.

In Fig. 1(b), as the probe beam coupled to the standing-wave cavity is reciprocating, we denote E_{it} and E_{ir} as the probe cavity-mode field copropagating and counterpropagating with the coupling field E_c, respectively. Figure 3 plots the real and imaginary parts of χ for the two cases in Fig. 2 in free space. The gray dotted lines in Fig. 3 are that of the two-level case ($\Omega_c = 0$). For the atom moving with a velocity v that feels the frequency detuning of E_{it} and E_c as $\Delta_p - kv$ and $\Delta_c - kv$, and the frequence difference between them is Doppler free, that is the two-photon resonance could be satisfied, then a sharp normal dispersion and a reduced absorption can be shown close to the center of atomic resonance, noted by the red dashed lines, that is the EIT effect. Conversely, however, the moving atom feels the frequency detuning of E_{ir} and E_c are $\Delta_p + kv$ and $\Delta_c - kv$, respectively, a Doppler shift with $2kv$ is created that is not satisfied with two-photon resonance. Here, the dispersion for the intercavity medium to E_{ir} is anomalous, and the strong absorption replaces the transparency for E_{ir} close to the center of the single-photon resonance, noted by the blue solid lines, which is the key factor that suppress the dark-state polariton in SC. In Fig. 3(b), note that the probe cavity mode neither co- or counterpropagates with the coupling field, and a Gaussian absorption profile is always present based on the Doppler background. The width and depth of the absorption profiles depend on the intensity of the coupling, and their absorptive centers are controlled by the coupling detuning.

Due to the difference in the susceptibility feature for the intracavity medium and the reciprocating cavity-mode fields, the intensity transmission function of the coupled atom-cavity system is given by

$$I = \frac{(1-r)^2 \exp(-\alpha_1 l)}{[1 - r\exp(-\alpha l)]^2 + 4r\exp(-\alpha l)\sin^2(\psi/2)}, \quad (4)$$

where r is the reflectivity of the mirrors, $\alpha = (\alpha_1 + \alpha_2)/2$, α_1 and α_2 are the absorption coefficients of intracavity atoms to E_{it} and E_{ir}, respectively; ψ is the cavity-mode round-trip phase shift and is described as

$$\psi = \frac{2\pi(\Delta_p - \delta_q)}{\Delta_{\text{FSR}}} + \frac{2\pi l}{\lambda}(n_1 + n_2 - 2), \quad (5)$$

where Δ_{FSR} is the free spectral region (FSR) of the near confocal cavity and l is the length of the Cs cell in the cavity, $n_{1(2)}$ is the refractive index, and $n_{1(2)} - 1$ is proportional to the dispersion of intracavity atoms to the $E_{it(r)}$.

If $\alpha_2 = \alpha_1$ and $n_2 = n_1$, then Eq. (4) describes the intensity transmission function of the RC. Using a lower atomic velocity distribution, Fig. 4 theoretically compares the normalized cavity transmission spectrum for SC and RC. Under the condition of atomic resonance ($\Delta_c = \delta_q = 0$), for RC, a narrow central dark-state peak (intracavity EIT) can be created obviously [see the dashed line (I) in Fig. 4]. For SC, however, the dark-state peak is seriously suppressed due to the strong absorption of the intracavity atoms to E_{ir} [see the solid line (II) in Fig. 4]; this coincides qualitatively with the experimental result in Fig. 2. Certainly, if the theoretical analysis is in agreement strictly with the experiment, more concrete parameters and factors should be considered on the modeling of this system.

For SC, when the coupling frequency deviates from the atomic resonance ($\Delta_c \neq 0$), it will not happen at the same position for the EIT effect caused by the intracavity medium copropagating E_{it} and the strong absorption of the counterpropagating E_{ir} due to the Doppler shift of the hot atoms (where the frequency difference is $2\Delta_c$), so the intracavity dark-state peak cannot be seen until the absorption effect becomes weakened.

It is found experimentally that the dark-state polariton peak can be generated obviously just when the coupling-field frequency deviates from the atomic resonance beyond $\sim \pm 100$ MHz within the interval of two normal sides under our experimental conditions. Since the absorption of the reflected cavity mode is still strong when the single-photon detuning Δ_c is smaller than 100 MHz, the
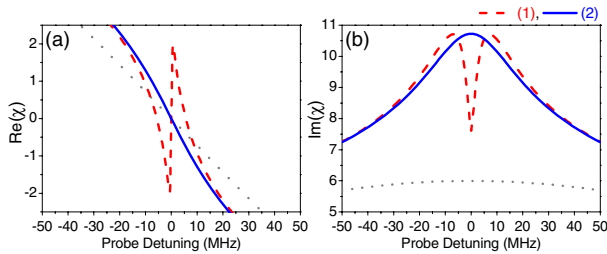

Fig. 3. (Color online) Theoretical calculations of (a) dispersion and (b) absorption curves versus the probe frequency detuning for the Doppler-broadened medium in different cases: (1) the probe copropagates with the coupling field (red dashed lines); (2) the probe counterpropagates without the coupling field (blue solid lines). $\gamma_{ca} = \gamma_{cb} = 2\pi \times 4.6$ MHz, $\gamma_{aa} = 2\pi \times 0.1$ MHz, $\Omega_p = 2\pi \times 2$ MHz, $\Omega_c = 2\pi \times 50$ MHz, $\Delta_c = 0$, and atomic density $N = 4.2 \times 10^{15}$ cm^{-3}.
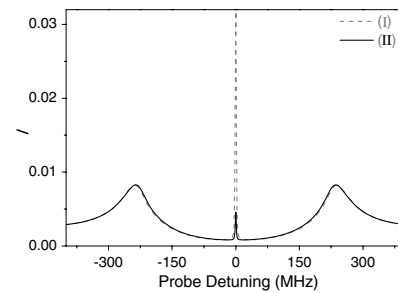

Fig. 4. Theoretical plots of the normalized cavity transmission function as a function of the probe frequency detuning for RC (I) (dashed line) and SC (II) (solid line). The parameters used in the calculation are: $r = 0.9$, $L \approx 150$ mm, $l = 75$ mm, and the other parameters are the same as in Fig. 3.

intracavity atoms are opaque to the probe mode in this range, which is dependent on the temperature of the intracavity atoms. Figure 5 presents the cavity transmission spectra versus the probe detuning at the different coupling and cavity-mode detunings. When the coupling frequency Δ_c is negatively detuned larger than 100 MHz at $\delta_q = 0$, a narrow intracavity dark-state polariton peak is created at the position of $\Delta_p = \Delta_c$, and its intensity rising with Δ_c is increased, see Figs. 5(a1) and 5(b1). The linewidth of the dark-state polariton peak is measured to be ~4 MHz, which is limited primarily by the composite cavity fineness in our experiment, and is smaller than that of the far-off resonance cavity mode (~24 MHz) and the EIT signal in free space (~13 MHz). Furthermore, when Δ_c is left detuned to superpose with the left normal mode, the intracavity EIT disappears and the left normal mode is splitting two sides [see Fig. 5(c1)]. The dashed lines are the relevent theoretical simulations, which are in reasonably agreement with the experimental results.

When the coupling detuning Δ_c is locked and shifting the cavity-mode frequency δ_q, the anticrossing-like behavior is shown for the position of the two normal side peaks, and has little influence on that of the dark-state polariton peak[19], but its transmission intensity is sensitive. For the specific Δ_c, the value of δ_q to achieve the max efficiency of the intracavity EIT peak is different. In Fig. 5(a2), when $\Delta_c = -116$ MHz, the max intracavity EIT is created at $\delta_q = -8$ MHz, just the increase is not obvious compared to the resonant center because of absolute intensity is small. For $\Delta_c = -185$ MHz, however, the max efficiency raises 1.5 times when δ_q is shifted to -70 MHz, meanwhile its linewidth remains unchanged, and its position is shifted left about 2 MHz at the large shifting range of δ_q due to the

pulling effect, as shown in Fig. 5(b2). At $\Delta_c = -232$ MHz, surprisingly, the intracavity EIT appears with efficient intensity and narrower linewidth when δ_q reached -120 MHz [see the solid line in Fig. 5(c2)]. That is because the frequency pulling effect of the cavity-mode detuning to the left normal mode is nearly linear with δ_q increased, whose frequency position is separated obviously from that of the intracavity EIT. Obviously, the shift value of δ_q to the maxium of the intracavity EIT is not in line with Δ_c detuned, which is mainly because the influence of δ_q on the intensity is asynchronous compared with Δ_c, as in Eq. (4). Note that it has some differences between the dashed line and the solid line in Fig. 5, because the bistability is generated for the normal mode in the experiment[18], but not considered in the theory.

In the experiment, on the basis of a guarantee to create dark-state polariton peaks, a profile with six peaks can be shown within one FSR by properly adjusting the experimental parameters. Figure 6 presents the experimentally measured cavity transmission spectrum at $\Delta_c = -176$ MHz. Comparing with Fig. 5(b2), one can see the similar change for the dark-state polariton peak with δ_q negatively detuned. In Fig. 6(d), at the resonant case ($\Delta_p = 0$), the central little peak is the residual resonant transmission, the left and right normal splitting modes split into two peaks, respectively. When the cavity mode is negatively shifted, for the left-hand normal mode peak, one of the split peaks moves outward and another moves inward [see Figs. 6(b)–6(d)]. When $\delta_q = -76$ MHz, the inward-moving peak merges with the central peak [see Fig. 6(a)]. For the right-hand normal mode peak, however, the two split peaks close gradually until merging into one peak [see Fig. 6(b)]. When the cavity detuning positively detuned, one can see the contrary result. Note that the influence of the dark-state polariton when $\delta_q = 48$ MHz shows a rather dispersive-
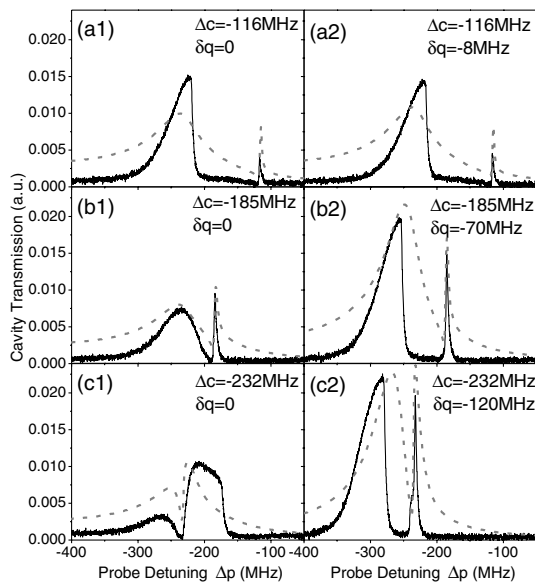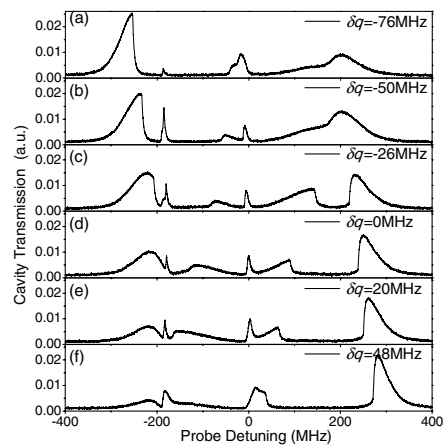

Fig. 5. The cavity transmission spectra versus the probe detuning at different coupling and cavity-mode detunings. The solid lines are the experimental measurement and the dashed lines are that of the theoretical simulation.

Fig. 6. Experimentally measured multipeak cavity transmission spectrum with $\Delta_c = -176$ MHz for different cavity-mode detunings. The experimental parameters are $T = 30$°C, $P_p = 4$ mW, and $P_c = 5$ mW.

like peak, not one merging peak as is shown for the left normal mode [see Fig. 6(f)].

In this Letter, we present our experimental investigations of the cavity transmission spectrum with hot three-level atoms coupled to an optical SC. Different from the result of the RC, the dark-state polariton peak is strongly inhibited at the atomic resonance due to the stong absorption effect of the counterpropagating cavity mode. When the coupling frequency is off resonance, a narrow linewidth dark-state polariton peak is created because the Doppler shift reduces the absorption of the counterpropating cavity mode. In theory, considering the coherent pumping factor, it can be qualitatively understood by plotting the dispersion and absorption properties of the probe co- and counterpropagating with the coupling field. Futhermore, the optimum positon of the cavity-mode frequency for the efficient dark-state polariton peak is theoretically and experimentally demonstrated. By changing parameters, a multipeak cavity transmission is observed experimentally. This study helps us to better understand the dynamic process of the coherent atoms coupled to the optical cavity system, which has potential applications in broadband, multichannel quantum information processing, and all-optical quantum devices.

References

1. G. Gabrielse, J. Tan, and P. Berman, *Cavity Quantum Electrodynamics* (Academic, 1994).
2. H. J. Kimble, Phys. Scr. T **76**, 127 (1998).
3. G. S. Agarwal, J. Mod. Opt. **45**, 449 (1998).
4. A. Boca, R. Miller, K. M. Birnbaum, A. D. Boozer, J. McKeever, and H. J. Kimble, Phys. Rev. Lett. **93**, 233603 (2004).
5. P. Maunz, T. Puppe, I. Schuster, N. Syassen, PW. Pinkse, and G. Rempe, Phys. Rev. Lett. **94**, 033002 (2005).
6. A. K. Tuchman, R. Long, G. Vrijsen, J. Boudet, J. Lee, and M. A. Kasevich, Phys. Rev. A **74**, 053821 (2006).
7. F. Brennecke, T. Donner, S. Ritter, T. Bourdel, M. Köhl, and T. Esslinger, Nature **450**, 268 (2007).
8. S. E. Harris, G. Y. Yin, A. Kasapi, M. Jain, and Z. F. Luo, Phys. Today **50**, 36 (1997).
9. J. G. Banacloche, Y. Q. Li, S. Jin, and M. Xiao, Phys. Rev. A **51**, 576 (1995).
10. M. Fleischhauer and M. D. Lukin, Phys. Rev. Lett. **84**, 5094 (2000).
11. A. Yang, C. Yan, J. Tian, C. Wang, G. Li, and D. Zhang, Chin. Opt. Lett. **11**, 051602 (2013).
12. D. Vitali, S. Gigan, A. Ferreira, H. R. Böhm, P. Tombesi, A. Guerreiro, V. Vedral, A. Zeilinger, and M. Aspelmeyer, Phys. Rev. Lett. **98**, 030405 (2007).
13. X. Zhong, G. Lin, F. Zhou, Y. Niu, and S. Gong, Chin. Opt. Lett. **13**, 092701 (2015).
14. S. F. Huelga, C. Macchiavello, T. Pellizzari, A. K. Ekert, M. B. Plenio, and J. I. Cirac, Phys. Rev. Lett. **79**, 3865 (1997).
15. W. Qi, Y. Jiang, X. Li, L. Jin, Z. Bi, and L. Ma, Chin. Opt. Lett. **14**, 101401 (2016).
16. G. Hernandez, J. Zhang, and Y. Zhu, Phys. Rev. A **76**, 053814 (2007).
17. H. Chen, K. Ying, Y. Duan, Y. Niu, and S. Gong, Chin. Opt. Lett. **12**, 092701 (2014).
18. M. Mücke, E. Figueroa, J. Bochmann, C. Hahn, K. Murr, C J. Villas-Boas, and G. Rempe, Nature **465**, 755 (2010).
19. H. B. Wu, J. Gea-Banacloche, and M. Xiao, Phys. Rev. Lett. **100**, 173602 (2008).
20. J. T. Sheng, H. B. Wu, M. Mumba, J. Gea-Banacloche, and M. Xiao, Phys. Rev. A **83**, 023829 (2011).
21. M. Albert, A. Dantan, and M. Drewsen, Nat. Photonics **5**, 633 (2011).
22. Z. P. Zhou, B. Yin, Q. Z. Deng, X. B. Li, and J. S. Cui, Photon. Res. **3**, B28 (2015).
23. L. Chen, C. M. Gao, J. M. Xu, X. F. Zang, B. Cai, and Y. M. Zhu, Opt. Lett. **38**, 1379 (2013).
24. L. Chen, Y. M. Wei, X. F. Zang, Y. M. Zhu, and S. L. Zhuang, Sci. Rep. **6**, 22027 (2016).
25. D. Liu, Q. Fan, M. Mei, J. Wang, Y. Pan, D. Teng, and J. Lu, Chin. Opt. Lett. **14**, 052302 (2016).
26. H. T. Zhou, D. W. Wang, D. Wang, J. X. Zhang, and S. Y. Zhu, Phys. Rev. A **84**, 053835 (2011).
27. P. Wang, J. Liu, F. J. Li, X. Shen, and R. X. Li, Photon. Res. **3**, 210 (2015).
28. J. T. Sheng and M. Xiao, Laser Phys. Lett. **10**, 055402 (2013).
29. H. X. Chen, Y. Q. Zhang, X. Yao, Z. K. Wu, X. Zhang, Y. P. Zhang, and M. Xiao, Sci. Rep. **4**, 3619 (2014).
30. X. D. Yu, M. Xiao, and J. Zhang, Appl. Phys. Lett. **96**, 041101 (2010).
31. K. Di, X. Yu, Y. Cheng, and J. Zhang, Chin. Opt. Lett. **10**, 091901 (2012).
32. J. Gea-Banacloche, H. B. Wu, and M. Xiao, Phys. Rev. A **78**, 023828 (2008).
33. C. Y. Ye and A. S. Zibrov, Phys. Rev. A **65**, 023806 (2002).